Phase equilibria and materials in the TiO$_2$–SiO$_2$–ZrO$_2$ system: a review

S. A. Kirillova[1,2], V. I. Almjashev[1,2,3], V. L. Stolyarova[1,4]

[1]I. V. Grebenshchikov Institute of Silicate Chemistry of RAS, Emb. Makarova, 2,
St. Petersburg, 199034, Russia

[2]St. Petersburg Electrotechnical University "LETI", Professor Popov St., 5,
St. Petersburg, 197376, Russia

[3]FSUE "Alexandrov Research Institute of Technology", Koporskoye sh., 72,
Sosnovy Bor LR, 188540, Russia

[4]St. Petersburg State University, Universitetskaya nab., 7/9, St. Petersburg, 199034, Russia

refractory-sveta@mail.ru, vac@mail.ru, stolyarova.v@iscras.ru

This paper analyzes the available data on phase equilibria in the TiO$_2$–SiO$_2$–ZrO$_2$ system. The advantages of specialized databases and software systems for the analysis of information on phase equilibria are pointed. Phase diagrams are kind of a roadmap for the design of materials. As shown in the review, nanomaterials are no exception to this. Data on phase equilibria, such as eutectic points, solubility limits, binodal and spinodal curves, make it possible to predict the possibility of the formation of nanoscale structures and materials based on them. In its turn during the transition to the nanoscale state, the mutual component solubility, the temperature of phase transformation may change significantly, and other features may become observable. This provides additional variability when choosing compositions and material design based on the phases of a given system. As an example, for design of nuclear fuel assemblies that are tolerant to severe accidents at nuclear power plants, mixed carbides (so-called MAX-phases) are considered as one of the most promising options as nanoscale layers on fuel cladding. It is suggested that the materials of the TiO$_2$–SiO$_2$–ZrO$_2$ system, which are the product of oxidation of some MAX-phases, can serve as an inhibitor of their further corrosion. Ensuring the stability of materials based on MAX-phases expands their prospects in nuclear power. This requires comprehensive information about phase equilibria and formation conditions of nanostructured states in the analyzed system.

Keywords: phase equilibria, zirconia, silica, titania, nanomaterials, MAX-phases, nuclear safety.

Received: 3 February 2021

Revised: 25 September 2021

1. Introduction

Nuclear power safety directly depends on the choice of reactor materials. The core materials are especially critical. In particular, the zirconium as a fuel cladding material, which has proven itself well under normal operating conditions, turns out to be extremely dangerous in beyond design basis accidents [1]. For this reason, there is an active search for a safer material to replace zirconium all over the world. One of these options is MAX-phases – a family of ternary layered compounds corresponding to the conditional formula M$_{n+1}$AX$_n$ ($n = 1, 2, 3, ...$), where M is a transition d-metal (Sc, Ti, V, Cr, Zr, Nb, Mo, Hf, Ta); A – p-element (Si, Ge, Al, Ga, S, P, Sn, As, Cd, I, Tl, Pb); X is carbon or nitrogen. These materials exhibit a unique combination of properties common to both metals and ceramics [2,3]. They are of low density; high thermal and electrical conductivity; high strength; excellent corrosion resistance in aggressive liquid media, resistance to high-temperature oxidation and thermal shock; easily machined; high melting point and are quite stable at temperatures up to 1000 °C and above [2–5]. That is, according to the combination of characteristics, the MAX-phases can be ideal for the fuel cladding material of nuclear reactors. However, the prospects of their use cannot be assessed without a comprehensive study of their stability, especially in the Nuclear Power Plants accident conditions. In this case, their unique features can be used to the full, leading to a decrease in the likelihood of severe accidents or, at least, to mitigate their consequences.

One of the aspects of such investigations is the study of the oxidation products of MAX-phases, in particular, zirconia, silica and titania. Materials based on these components, presenting certain combinations of phases and features of their dimensional parameters and mutual arrangement, can both contribute to the destruction of claddings based on MAX-phases and serve as good protectors against their further corrosion. To assess the boundaries of stability and predict the properties of these materials, it is necessary to know the phase equilibria in the TiO$_2$–SiO$_2$–ZrO$_2$ system, as well as to know the features of the formation of structures that have the physicochemical and mechanical properties necessary to create a protective layer.

So, for example, on the basis of the system under consideration, the formation of nested glass-crystalline structures is possible. Interest in materials with a hierarchically organized spatial distribution of phases, including nanostructured materials, is associated with their unique characteristics. For such materials, it becomes possible to fine-tune their properties in a very wide range [6–9].

The study of the formation of hierarchical structures deserves special attention. One of these processes is phase decay and, in particular, separation in the liquid phase – miscibility gap [10–20]. The structures that appear upon rapid cooling of samples from the miscibility gap can be classified as hierarchical due to the appearance of a number of sublevels with rounded inclusions ranging in size from 0.01 to 10 μm [11].

Materials with a hierarchical structure arising during the crystallization of immiscible viscous oxide liquids can be classified as nanomaterials containing nanosized blocks (crystallites) at the lowest levels of the hierarchy, included in a glassy or crystalline matrix [7]. In addition to the size factor, the shape and spatial distribution of phases have a significant effect on the properties of such materials. The hierarchical structure formed during the cooling of immiscible melts is associated with the boundaries of phase stability and reflects the history of the decay of primary and formation of secondary phases [21]. This determines, as a rule, the characteristics of the materials thus formed [18, 19, 22–25].

Thereby, to solve the problem of creating and studying the physicochemical features and stability of materials, it is necessary to analyze the available information on phase equilibria. In the review, we are performed such an analysis for the TiO_2–SiO_2–ZrO_2 system. It also provides information on materials based on the TiO_2–SiO_2–ZrO_2 system and their relationship with data on phase equilibria.

2. TiO_2–SiO_2 system

The TiO_2–SiO_2 system is important for interpreting the interaction of titanium and silicon dioxides in the production of ceramics, glass ceramics, and glasses. Based on the components of the system, it is possible to create fundamentally new materials with unique mechanical, optical and catalytic properties [26–37]. In addition, the components of the system themselves have a variety of properties that are promising for modern technology [38–40].

The data given in the literature on the TiO_2–SiO_2 system are contradictory [4, 41–43, 45–53]. In particular, the authors of [41–43] carried out experiments in a reducing atmosphere, and in this connection, possibly, in addition to TiO_2, the samples contained the oxides Ti_2O_3 and Ti_3O_5. The authors of [42] found that this system is characterized by the presence of a region of immiscibility of two liquid phases, which was not noted in [44]. In [45], contrary to previous studies, two series of solid solutions were found in the system, the existence of which was not confirmed later in [46]. The authors of [46] clarified the position of the eutectic point defined in [44]. According to those authors [46], the eutectic in the TiO_2–SiO_2 system corresponds to a composition of 8.1 mol. % TiO_2 and a temperature of 1550±4 °C. In [46], data on the position in the system of the region of immiscibility of two liquid phases arising at 1780±10 °C in the range from 15.0 to 90.9 mol. % TiO_2, i.e., significantly different from the data of [42].

Other research [47] shows the calculated diagram of the state of the system obtained on the basis of previously published data on phase equilibria in the system and thermodynamic data on SiO_2 and TiO_2 [48]. It is noted that the experimental data on the boundaries of the region of immiscibility of two liquid phases are unknown, and the critical point of the miscibility gap is 56.3 mol. % TiO_2 and 2618 °C, was obtained only from the data of thermodynamic modeling of the region of immiscibility of liquid phases. In addition, the existence of solid solutions from the side of TiO_2 is taken into account. It should be noted that the work [47] used an approach based on combining the available experimental information for phase equilibria and thermodynamic properties of the phases of the system. Then it is describing the properties of each phase by a mathematical model containing a set of tunable parameters, and carrying out the procedure for finding the parameters of the phase models that best suit all available information about the phase equilibria of the system of interest to the researcher. This approach has become widespread and has actually become the standard for thermodynamic optimization of phase diagrams. In the literature, the method has the abbreviation CALPHAD (from the CALculation of PHAse Diagrams) [54].

In works [49, 50] on the basis of experimental data [46, 51–53] and their own data on the boundaries of the region of immiscibility of two liquid phases, a variant of the thermodynamically optimized diagram of phase equilibria in the TiO_2–SiO_2 system based on the sub-regular model was proposed. In the case when the thermodynamic parameters of the used model are taken to be independent of temperature, the critical point of the miscibility gap is 50.8 mol. % TiO_2 and 2374 °C, and for the linear dependence of the model parameters on temperature – 54.7 mol. % and TiO_2 2339 °C.

In [55], the eutectic and monotectic nature of the phase diagram of the TiO_2–SiO_2 system was confirmed by the Differential Thermal Analysis method (DTA) on an original setup. The temperature of the eutectic (1543±3 °C) and monotectic (1780±7 °C) transformations has been specified. The temperature of the eutectic is somewhat at odds with the previously obtained literature data, however, in general, it can be considered that the experimental data are in good agreement with the previously obtained results in [44, 46]. Scanning electron microscopy proved the presence

of a region of two immiscible melts. The data obtained for the temperature of monotectic transformation coincided with the results of [46], and the results for the liquidus line above the monotectic temperature also do not contradict them. Based on the coordinates of the liquidus line and the points of invariant transformations, the parameters of the model of subregular ionic solutions [56] for melts of the TiO$_2$–SiO$_2$ system were determined and a thermodynamically optimized phase diagram was constructed in the temperature range of 1500–1900 °C.

In [57], phase equilibria in the TiO$_2$–SiO$_2$ system in the region of liquid phase separation were experimentally investigated. It is shown that in the experimental study of silicon-containing immiscible melts, an important factor that determines the microstructure and complicates the interpretation of the data is the dynamics of system cooling. Along with the rate of cooling of the melt, it is necessary to take into account such parameters of the system as the viscosity and density of coexisting liquid phases, diffusion of components, etc. Thus, for a melt based on SiO$_2$ at temperatures below monotectic, due to high viscosity, the liquid phase is slowly freed from the solid phase based on TiO$_2$, and at temperatures above monotectic, the release of the liquid phase from TiO$_2$ occurs at a significantly higher rate. Also, the work carried out a critical analysis of the available and obtained experimental data. A thermodynamically optimized phase diagram of the TiO$_2$–SiO$_2$ system based on the model of subregular solutions has been constructed. The phase diagram obtained by optimization by the CALPHAD method differs markedly from the diagram given in [50], which was constructed using experimental data on the composition of liquid phases at the boundary of the miscibility gap at temperatures significantly higher than the monotectic temperature. Apparently, in [50], the microstructure of samples quenched from temperatures of 2185 and 2260 °C was unreasonably interpreted as corresponding to the state of equilibrium immiscibility at these temperatures (Fig. 1*a*). Such a character of the microstructure may be a consequence of the decomposition of a homogeneous melt during quenching. This assumption is supported by the fact that a uniform pattern of phase decomposition is observed over the entire volume of the sample.
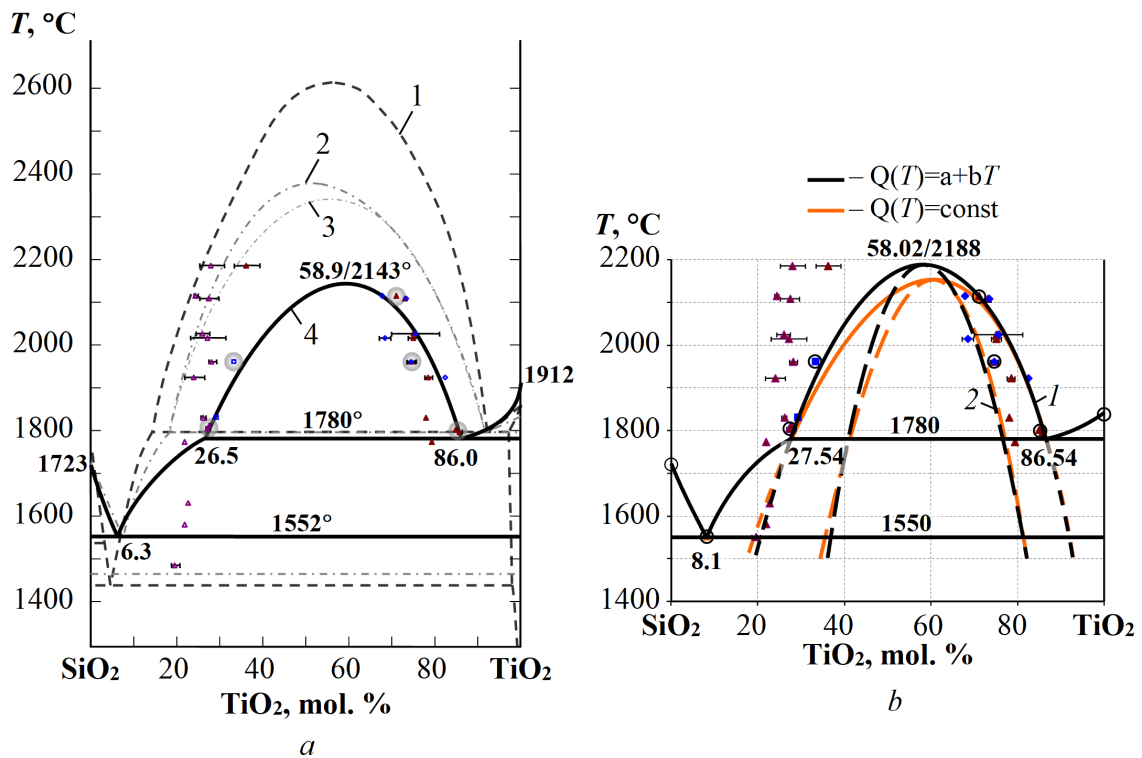

FIG. 1. Phase diagram of the TiO$_2$–SiO$_2$ system: *a* – 1 – [47], 2 – [49], 3 – [50], 4 – [57]; *b* – [58]:
1 – binodal curves; *2* – spinodal curves

In [58], on the basis of experimental data obtained in [57], the parameters of the subregular melt model were determined without and taking into account the temperature dependence of the mixing energies of the components. Using the obtained parameter values, as well as thermodynamic data for the pure components [59–61], and taking into account the absence of miscibility of the components in the solid phase, the binodal and liquidus lines in the TiO$_2$–SiO$_2$ system were constructed. On the basis of the obtained thermodynamic model, the curves of spinodal decomposition of the liquid phase were also constructed (Fig. 1*b*). Comparison of the experimental data with the curves of binodal separation and spinodal phase decomposition showed that, upon rapid cooling of the melt, the phase

decomposition in the liquid-phase region proceeds according to the spinodal mechanism [48] with the formation of materials with a hierarchically organized structure down to the nanometer scale. There are at least three levels of the hierarchy (Fig. 2). Thus, there is a fundamental possibility of experimentally constructing the spinodal of the system from data on the composition, shape, and spatial distribution of the solid regions of the phases over the volume of the material, obtained upon rapid cooling of the melt from the region of existence of two immiscible liquids.

In addition to determining the boundaries of phase equilibria and the features of phase separation and decomposition during cooling of immiscible oxide liquids in the TiO_2–SiO_2 system, the dependence of the microstructure on heating and cooling conditions was investigated. The results of the studies performed indicate that the parameters of the microstructure can be controlled at all levels of the hierarchy.

The authors of [63] draw attention to the fact that in the phase diagram of TiO_2–SiO_2 system, there are large discrepancies between the calculated and experimental data (Fig. 3). They suggest that these discrepancies are likely due to inherent difficulties in the system: the need to operate in an inert atmosphere to avoid the formation of Ti_2O_3 and Ti_3O_5, and the high temperature problems associated with miscibility gap and high SiO_2 content. For example, in [46], it is indicated that difficulties arose with the determination of the eutectic in the SiO_2-rich region, since it was impossible to reach equilibrium due to the high viscosity and the steep slope of the liquidus. In [57], the importance of the quenching rate for obtaining equilibrium data is also indicated. In general, it is necessary to implement new approaches for further experimental studies that will allow confirming the equilibrium data. As indicated, the experimental data from [57] are closest to the calculations. The critical temperature of the miscibility gap in the TiO_2–SiO_2 system is closer to [57]. The melting point of rutile is higher than that taken from [64]. The run of the liquidus curve correlates well with the new values from the Scientific Group Thermodata Europe (SGTE) substance database. Deviations from monotectic and eutectic points have not yet been explained and should be further investigated. The line going from pure rutile to the eutectic at 9 mol. % SiO_2 is parallel to that in [46] and the eutectic temperature is also higher than the experimental one. The calculated liquid level decreases towards SiO_2 enrichment. The discrepancy can be explained by the experimental difficulty in establishing equilibrium, and the kinetics can be very complex for such viscous compositions. The absence of the SiO_4^{4-} ion is notable. The SiO_4^{4-} ion is usually present in most oxide binary systems MO_x–SiO_2. However, in the case of the TiO_2–SiO_2 system, according to the experimental phase diagram, there is a wide region of immiscibility between TiO_2 and SiO_2. This indicates that TiO_2 does not participate in the destruction of the SiO_2 network, and does not use it together. In the model proposed in [49], liquid TiO_2 is described as $Ti^{4+} : O^{2-}$, where the addition of TiO_2 to SiO_2 does not destroy the oxygen bridge of SiO_2. Thus, there is a metastable miscibility gap between TiO_2 and SiO_2.

In [63], calculated data on the activity of SiO_2 in the TiO_2–SiO_2 system at 1527, 1627, and 2527 °C are also presented. Unfortunately, there is only one experimental point at 1627 °C for the $TiO_2 : SiO_2$ molar ratio of 1 : 1 [65]. A strong positive deviation from ideality and the inflection point of the liquidus arises due to the presence of liquid phase separation (Fig. 3).

The concepts of the nature of immiscibility in the TiO_2–SiO_2 system, opposite to those of [63], are given in [66]. Thermodynamic/dynamic modeling of liquid immiscibility in silicate systems is seriously hampered by the lack of *in situ* studies of the structural evolution of the melt. In work [51], the structural evolution at the atomic level of the TiO_2–SiO_2 system with a miscibility gap is studied by in situ high-energy X-ray diffraction. The authors suspended 10 mg fragments of sintered at 1000 °C ceramics in a stream of pure oxygen and melted with a CO_2-laser. Samples were overheated up to 2300 °C, then they were quenched to the target temperature, and the droplet was stabilized for 20–30 s and the diffractometric data were collected for 15 s. In the opinion of the authors, this was sufficient to avoid a strong drift of the composition due to the evaporation of SiO. For a composition of 30 mol. % TiO_2, a homogeneous liquid was assumed by the authors at a level of 2220 °C. At 1950 °C, according to their data for a composition of 30 mol. % TiO_2, a heterogeneous state was observed. At 1600 °C there was a metastable miscibility gap. Authors did not carry out measurements between these temperature levels. They chose the composition and temperature based on one of the versions of the phase diagram [46]. The authors, taking the work [46] as a basis, did not take into account other data [57, 58, 63], which can significantly affect the processing of their data and conclusions.

It was found that both the configuration of the [SiO] monomers and the polymerization between them are closely related to the incorporation and extraction of metal cations (Ti^{4+}). The [SiO] monomer undergoes oxygen-deficient polymerization and over-polymerization before liquid-liquid separation and self-healing after liquid-liquid separation, thus challenging the traditional concept of unchanged monomer [SiO_4].

Ti^{4+} cations with tetrahedral oxygen coordination first participate in the formation of the network before liquid separation. The four-fold Ti–O bond breaks during liquid separation, which can facilitate the movement of Ti^{4+} through the Si–O network to form TiO_2-rich nodules. The structural features of the nodules were also investigated and found to be very similar to those of the TiO_2 melt, suggesting parallel crystallization behavior in the two cases. The authors [66] hope that their results will allow one to see the structural evolution of immiscible liquid phases on
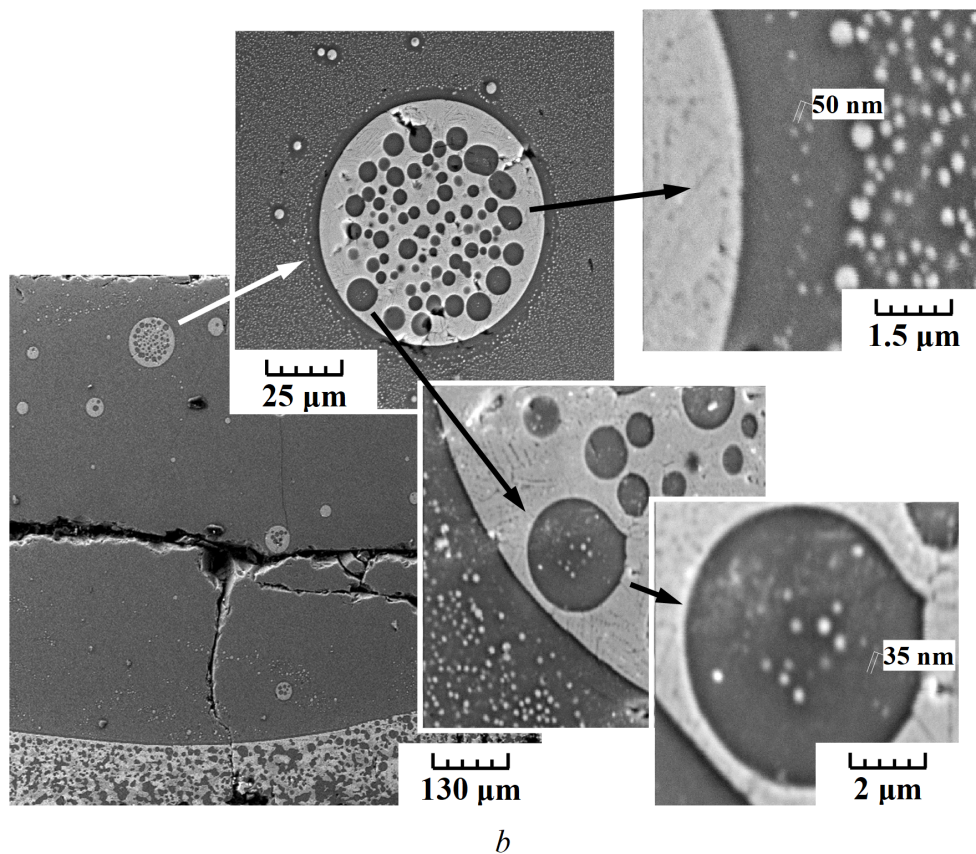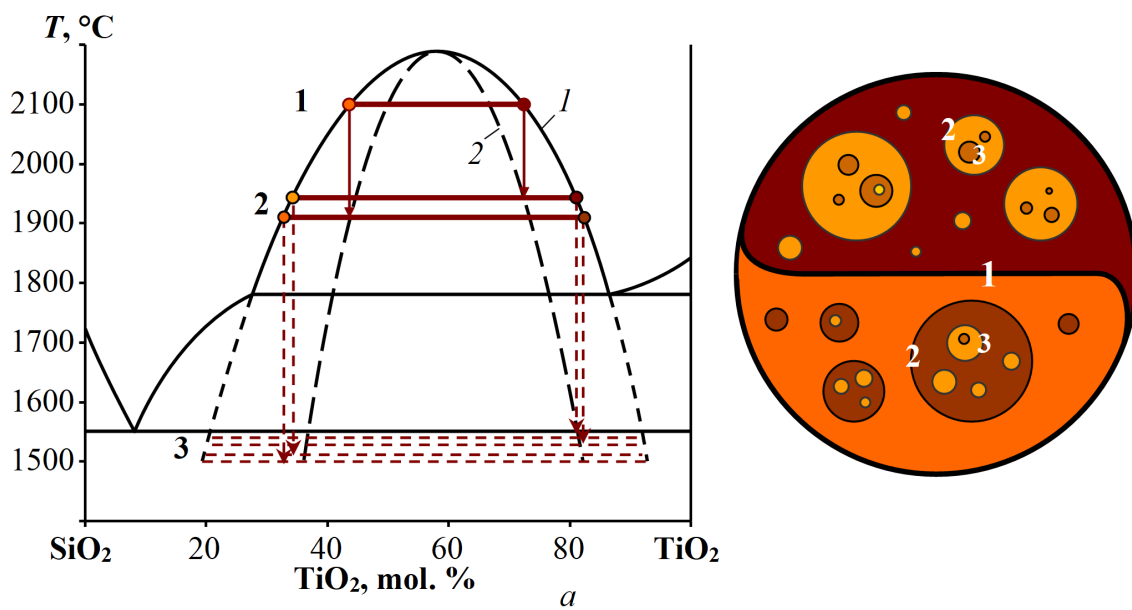
FIG. 2. Formation of a multilevel hierarchical microstructure in the process of spinodal decomposition of immiscible oxide liquids [58]: *a* – scheme of the phenomenon: *1* – binodal separation curve and *2* – spinodal decomposition curve; **1**, **2**, **3** – levels of the structural hierarchy, *b* – hierarchically organized microstructure in the TiO₂–SiO₂ system
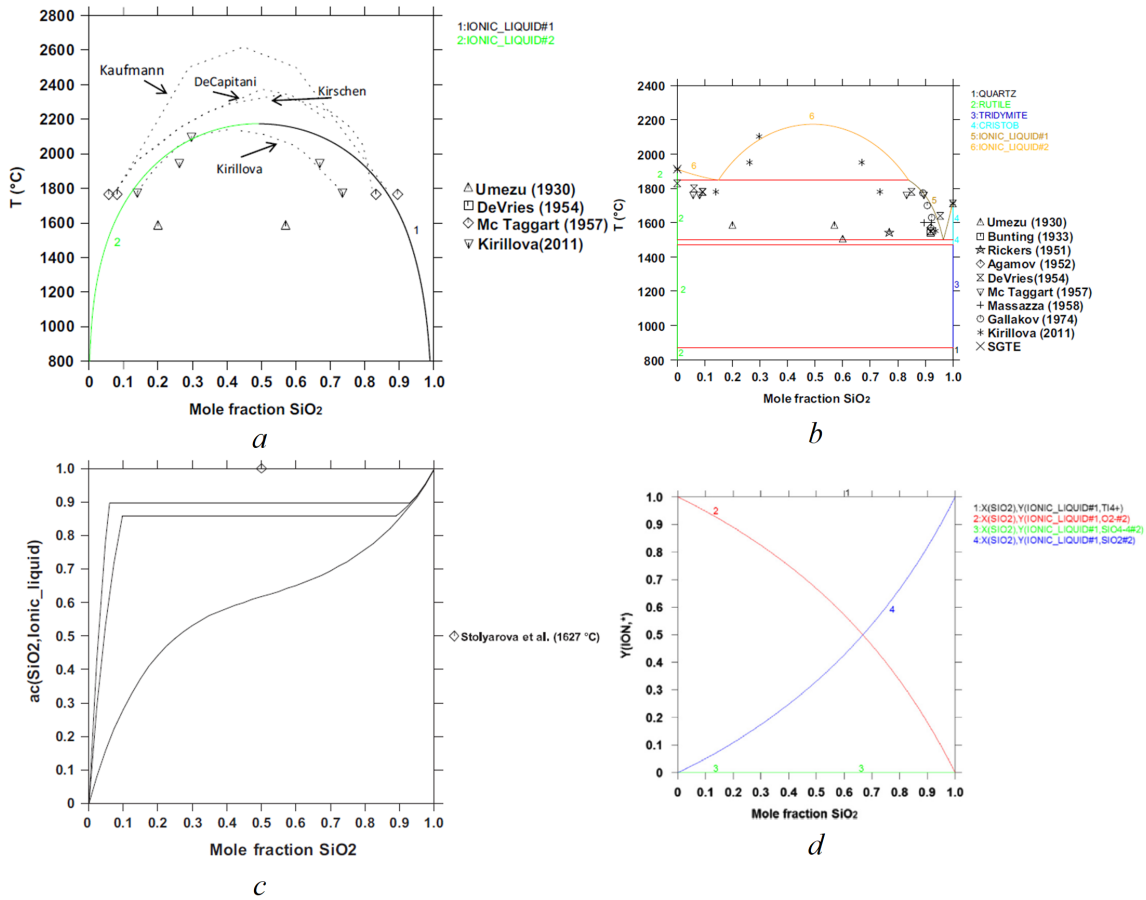
FIG. 3. Immiscibility thermodynamic analysis in the TiO_2–SiO_2 system taken from [63]: a – calculated miscibility gap, experimental data and models; b – calculated miscibility gap, liquidus, terminal phases and experimental data; c – SiO_2 activity at 1527, 1627 and 2527 °C, experimental point at 1627 °C; d – Y_{ion} for SiO_2, SiO_4^{4-}, O^{2-} species at 2727 °C

an atomic scale, which will contribute to the construction of a complete thermodynamic/dynamic structure describing systems of silicate immiscibility in the liquid phase outside of existing models.

Thus, despite a large number of studies on phase equilibria in the TiO_2–SiO_2 system, there are a number of conflicting information on the position of the phase equilibrium lines that require additional analysis, experimental and calculated refinements.

3. TiO_2–ZrO_2 system

Phase formation in the TiO_2–ZrO_2 system was studied in a number of works [67–98], but only the high-temperature region of the phase diagram is described in detail, as a rule, above 1000–1200 °C. There are very few studies of the behavior of this system in the low-temperature region, as well as those taking into account the particle size of the components. At the same time, for the creation of new materials, including those based on TiO_2–ZrO_2 composites, nanosized compositions can be promising, the reactivity, behavior, structure and properties of which are determined to a large extent by the sizes of their constituent particles [99–105].

The data obtained in [104] show that the nucleation process limits chemical transformations in the low-temperature region in the system under study. The formation of a compound of variable composition $(Zr,Ti)_2O_4$ with a fluorite structure at low temperatures is caused by the formation of the hydroxocomplex $[Zr(OH)_2 \cdot 4H_2O]_4^{8+}(OH)_8^{-}$ in the structure of which Ti^{4+} ions are dissolved at the stage of precipitation. Moreover, the limiting substitution of Zr^{4+} ions for Ti^{4+} ions in the amorphous hydroxocomplex is significantly lower than 45 mol. %. Thus, the results obtained in this work confirm the promise of an approach to the control of solid-phase chemical transformations and phase transformations in nanostructured systems based on the formation of pre-nucleus clusters with a given structure (see, for example, [106, 107]).

It was noted in [105] that there are significant inconsistencies between the versions of the TiO$_2$–ZrO$_2$ phase diagrams regarding the structure and phase field of the existence of zirconium titanate, especially at low temperatures. As a result, a detailed study of the formation of zirconium titanate was carried out. ZrTiO$_4$ nanocrystals with a skrutinite structure (α-PbO$_2$) were obtained by coprecipitation followed by calcination in air. Phase formation was studied in the temperature range 25–1100 °C using simultaneous thermal analysis, high-temperature diffractometry, and scanning electron microscopy. It was found that crystallization of ZrTiO$_4$ occurs at temperatures above 700 °C after complete removal of water. Nanoceramics based on ZrTiO$_4$ were obtained by sintering the nanopowder at 1200 °C for 5 hours. The thermophysical characteristics of the obtained nanodispersed ceramics were measured using laser pulse analysis and thermomechanical analysis. The resulting ceramics exhibit improved thermal insulation properties (α = 0.138–0.187 mm^2/s, λ = 5.446–11.512 W/(m K)) and a low coefficient of thermal expansion (CTE = (3.45–7.38) $\times$ 10^{-6} K^{-1}) in the temperature range 25–800 °C. This makes the resulting nanoceramics promising as a material for creating thermal barrier coatings.

Fig. 4 shows the known experimental versions of the phase diagrams of the TiO$_2$–ZrO$_2$ system. It is easy to see that the data on phase equilibria are replete with discrepancies, both in the region of the solubility of the components in each other, and in the field of the formation of compounds, their nature and character.

It should be noted that in [67] the liquidus curve is shown with the eutectic in exact accordance with the historically first constructed phase diagram [70] (Fig. 4a, red lines). Compounds formation was not found in [68]. The phase diagram published in [69] shows the absence of compounds and eutectics at 45–50 mass. % TiO$_2$ and 1600 °C.

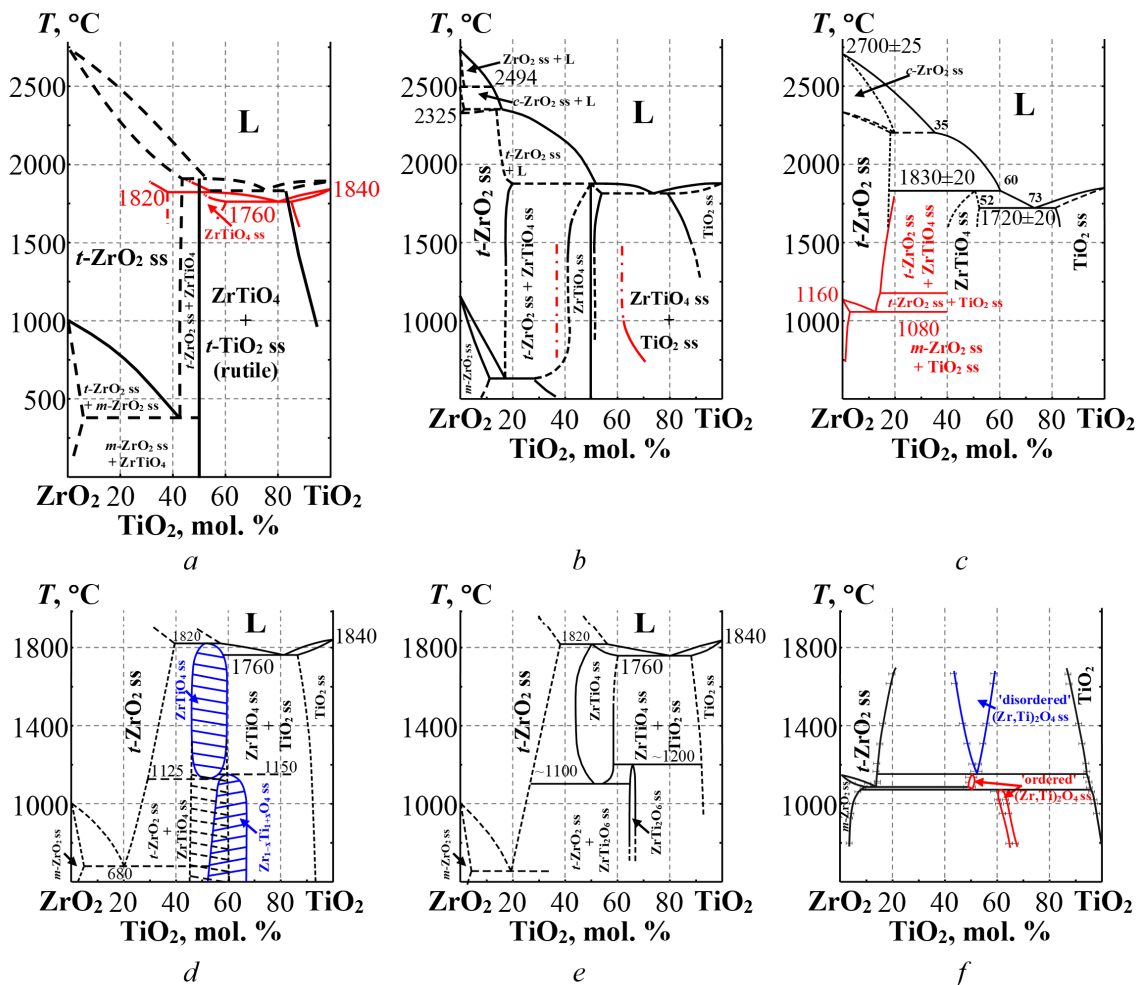FIG. 4. Phase diagram of the TiO$_2$–ZrO$_2$ system (experimental study): a – red line [70], black line [71], b – black line [72, 73, 75, 85], red line [88], c – red line [78], black line [79], d – [81, 82], e – [83], f – [96]; ss – solid solution, m-, t-, c- – monoclinic, tetragonal and cubic polymorph, respectively, L – liquid

In [71], fourteen compositions were prepared from zirconium dioxide with impurities less than 1 % and anatase. The samples were mixed, compressed into tablets and heated for two hours in an oxygen-acetylene oven with excess O_2 at 1760 °C. After that, they were heated in an electric resistance furnace at 1370 °C for 336 hours and at 980 °C for 1465 hours. The phases were determined using X-ray diffractometry. The plotted phase diagram (Fig. 4*a*, black lines) does not include the cubic form of the ZrO_2 solid solution or the $ZrTi_2O_6$ phase.

The system has been extensively researched and the phase diagram (Fig. 4*b*, black lines) reproduced the results of other studies [72, 73, 75, 85]. In [72], ZrO_2 (with 2 mass. % HfO_2 and without other spectrographically observed impurities of more than 0.05 %) and TiO_2 (with 1.5 mass. % SiO_2 and without other spectrographically observed impurities of more than 0.005 %) was used. They investigated the solid solution boundaries between ZrO_2 and $ZrTiO_4$, the effect of the TiO_2 solid solution on the monoclinic-tetragonal transition of ZrO_2, and the TiO_2 solid solution boundary. The following analytical methods were used: X-ray diffraction at elevated and room temperatures and electrical conductivity.

In [75, 85], using ZrO_2 with a purity of 99.8 %, including 1.8 mass. % HfO_2 and TiO_2 with a purity of 99.7 %, 18 liquidus points were determined from the solar heating and rapid cooling curves. The temperatures measured by the brightness pyrometer were considered with accuracy up to ±20 °C at 2700 °C and ±15 °C at 1700 °C. In addition, 25 compositions quenched in air from the melt, as well as from 1700 °C were studied by X-ray diffractometry. High temperature X-ray diffractometry was also used on the ZrO_2 rich side to determine the boundaries of the solid solution below 1200 °C. As for the maximum degree of a tetragonal solid solution, the data [75,85] agree with the data [72–74], but differ somewhat from other studies.

The agreement for the lowest transition temperature between monoclinic and tetragonal ZrO_2 is poor. In [75, 85], the dependence of the unit cell parameters on the composition for solid solutions based on ZrO_2, $ZrTiO_4$ and TiO_2 are presented. They also offer a fourth form of ZrO_2 that is stable above 2494 °C, but this is doubtful as it is based solely on small kinks in the rapid cooling curves.

Although other studies [72–75, 85] agree with the end terms of solid solutions and one solid solution based on an intermediate compound, some details of phase equilibria remain a big question.

In [70], the starting materials were dense ZrO_2 with a nominal purity of 99 % and highly purified TiO_2 with a purity of >99.9 %. Samples for 16 compositions were mixed with a binder and compressed into tablets, which were then annealed in air for 4 hours at 1200 °C on Pt foil. After cooling, the samples were crushed, pressed, and annealed for 4 h at 1350 °C in air. X-ray examination showed that the solid phase reactions were completely done. The tablets were then ground, mixed again with the binder, compressed into tablets, from which small four-sided pyramids were ground. These pyramid samples were heated in an oven with resistance heaters and thorium oxide lining with an oxidizing atmosphere to determine the solidus and liquidus temperatures. The rounding of the corners of the pyramids was taken as the temperature of the solidus, and the complete melting was taken as the liquidus. Cooled fused samples and others quenched at temperatures up to 1600 °C were studied petrographically and by X-ray diffraction. The X-ray diffraction pattern of $ZrTiO_4$ powder is indexed as a rhombic phase.

In Fig. 4 (*b*, red lines) show the phase diagram of the TiO_2–ZrO_2 system according to [88]. The precursors were prepared by the sol-gel method, heated to 800 °C, and held at that temperature for 10 h. The products were studied by X-ray diffraction and DTA. Metastable solid solution based on $ZrTiO_4$ is shown by dash-dotted lines. The main diagram is taken from [76] (Fig. 4*b*, black lines).

In [78], analytically pure ZrO_2 and TiO_2 were used as starting materials. The pressed powders were heated in an electric resistance oven for 168 hours. The samples were examined by DTA and X-ray diffractometry. It was found that the ZrO_2 tetragonal solid solution undergoes eutectoid decomposition at 1080 °C. The monoclinic to tetragonal transition of ZrO_2 occurs at 1160 °C and the tetragonal to cubic transition at 2300 °C. The data obtained are shown as a refinement on a fragment of the phase diagram (Fig. 4*c*, red lines).

Twenty-five compositions were prepared from ZrO_2 and TiO_2 of high-purity qualification, pressed into tablets, and heated in a gas (air) furnace at 1700 °C in corundum crucibles in [79]. Sintering and thermal analysis were carried out on air in a solar oven. DTA in a He atmosphere was used to determine the temperatures of formation of $ZrTiO_4$ and eutectic. The phases were studied by X-ray diffraction and microstructural analysis. At 1700 °C, there is a single-phase region of tetragonal zirconia up to about 17.5 mol. % TiO_2, a single-phase solid solution $ZrTiO_4$ from ~40 to 52 mol. % and a rutile-based solid solution TiO_2 from about 82.5 mol. %. Cooling curves of pure ZrO_2 and ZrO_2-based solid solutions show that cubic ZrO_2 transfers to the tetragonal form at 2330±25 °C and the transition temperature is reduced to 2190 °C by adding TiO_2. The unit cell sizes of various solid solutions are reported. Phase diagrams are constructed (Fig. 4*c*, black lines).

The subsolidus region of the system has attracted and continues to attract close attention of researchers. In papers [81, 82], preliminary data on phase relations are given for the system. The experimental data also are focused around the $ZrTiO_4$ compound. Pure (unalloyed) powders were prepared using alkoxide precursors. It was found that $ZrTiO_4$

solid solutions undergo an order-disorder phase transition, and the phase below $\sim$1125–1150 °C is only metastable (Fig. 4*d*, dashed lines). The stable phase at temperatures below $\sim$1150 °C is the solid solution $Zr_{1-x}Ti_{1+x}O_4$. This phase has an incommensurate superstructure, and its structure based on $Zr_5Ti_7O_{24}$ was described in [84]. Evidence for a phase transition in $ZrTiO_4$ was included in [81, 82].

The phase relations in the TiO_2–ZrO_2 system in [83] were investigated near the $ZrTiO_4$ compound by means of an experimental study, including the characterization of both single-crystal and powder samples. Since $ZrTiO_4$ melted incongruently at 1820 °C, it could not be grown directly from the melt of its own composition. Therefore, growth methods using a flux were used [77]. Conventional ceramic powders with particle sizes several orders of magnitude larger than powdered alkoxide precipitates were obtained by solid-phase reaction of high-purity TiO_2 (anatase) and low-hafnium ZrO_2. Several cycles of prolonged thermal treatment at $\sim$1500 °C with grinding between heat treatments were necessary for the complete reaction to proceed until a homogeneous solid solution was obtained.

The total number of heat treatments varied from $\sim$3–7 for different compositions. In the case of some compositions, doping with 0.5 mol. % Y_2O_3 was carried out to accelerate the kinetics of phase transitions in order to achieve phase equilibrium in studies. Some compositions were prepared by coprecipitation of a mixed metal alkoxide solution using zirconium n-butoxide $[Zr(OC_4H_9)_4]$ and titanium isopropoxide $[Ti(OC_3H_7)_4]$ as starting materials and toluene as solvent. The sediment was X-ray amorphous. The average particle size of the agglomerates was from 1.0 to 0.05 μm, and the BET surface area was 350 m^2/g, corresponding to a particle size of 10.5 nm. These powders crystallized at temperatures above 450 °C to a metastable single-phase structure. To achieve true structural equilibrium, prolonged annealing (over 1 month) at temperatures from 500 to 1000 °C was required. Powder X-ray diffraction, neutron powder diffraction, and X-ray diffraction studies on a single-crystal precession chamber were used to characterize the structure of various solid solutions of zirconium titanate prepared and thermally-treated for research.

The presented unit cell parameters were obtained from the refinement of X-ray powder diffraction data using the least squares method [77], with additional refinement using multiple regression analysis to determine the disproportionate vector (intermediate degrees of the *a*-axis superstructure observed during a continuous phase transition from high to low temperature forms of zirconium titanate) when appropriate. The existence of the new compound $ZrTi_2O_6$ as a stable low-temperature phase was confirmed by the recently published discovery of the mineral srilankite [80], which has the same nominal composition and structure. The lattice parameters reported for the new mineral are in good agreement with the results of experiments on low-temperature crystallization at 650 °C using coprecipitated powders. The wide range of solid solution from 35 to 75 mol. % TiO_2 was the result of metastable crystallization at low temperature of the high-temperature disordered α-PbO_2 polytype, and the single-phase field was much wider than the equilibrium region at high temperatures. It was found that minor impurities play a large role in the kinetics of the order-disorder transition in zirconium titanate compositions. The addition of 0.5 % Y_2O_3 to compositions for high-temperature synthesis leads to the fact that the cell of tripled phase, leading to a phase with a Zr : Ti ratio of $\sim$5 : 7, is in equilibrium with cubic ZrO_2 and $Y_2Ti_2O_7$ pyrochlore. The authors revised the earlier phase diagram of the system represented on Fig. 4*d* to include this new information (Fig. 4*e*).

Fig. 4*f* shows the TiO_2–ZrO_2 phase diagram constructed from experimental data in the range from 800 to 1200 °C (1 atm) [96]. The data above 1200 °C correspond to the data of [92]. The temperature range under consideration was previously inaccessible for equilibrium experiments due to the kinetic features of crystallization of $(Zr,Ti)_2O_4$. The crystallization of the ordered phase from the oxides was facilitated by the addition of a flux (CuO or Li_2MoO_4/MoO_3), and seeds. Note that all phases (tetragonal and monoclinic ZrO_2, ordered and disordered $(Zr,Ti)_2O_4$, TiO_2) are solid solutions, and the phase fields are marked with a predominant end member of the corresponding series. No distinction is made between partially or fully ordered $(Zr,Ti)_2O_4$, and the "ordered" label includes both partially and fully ordered $(Zr,Ti)_2O_4$ in this study.

The method of synthesis at high pressures with flux and seeds, developed previously [93, 94], was successfully applied for synthesis at atmospheric pressure and effectively ensured phase equilibria in the ZrO_2–TiO_2 system at temperatures below 1200 °C. Thus, the phase diagram extended by 400 °C differs from previously published works in that the composition of ordered $(Zr,Ti)_2O_4$ depends more on temperature than is constant [83, 89]. Moreover, the authors of [96] did not find evidence of the previously proposed two-phase field of the coexistence of ordered and disordered $(Zr,Ti)_2O_4$ [97]. Rather, the onset of the ordered transition was marked by the stability of the $(Zr,Ti)_2O_4$ phase with a composition ($x_{Ti} = 0.495$), which differs both from the disordered $(Zr,Ti)_2O_4$ above 1160 °C and from the ordered $(Zr,Ti)_2O_4$ below 1060 °C. Thus, the two different ordered phases differ in composition. Nevertheless, it was noted in [96] that detailed studies are needed to determine their exact ordering [86].

Many attempts have been made at the thermodynamic optimization of the phase diagram of the TiO_2–ZrO_2 system (Fig. 5). But since there is a wide variety of experimental material, the calculated versions of the diagram also differ greatly.
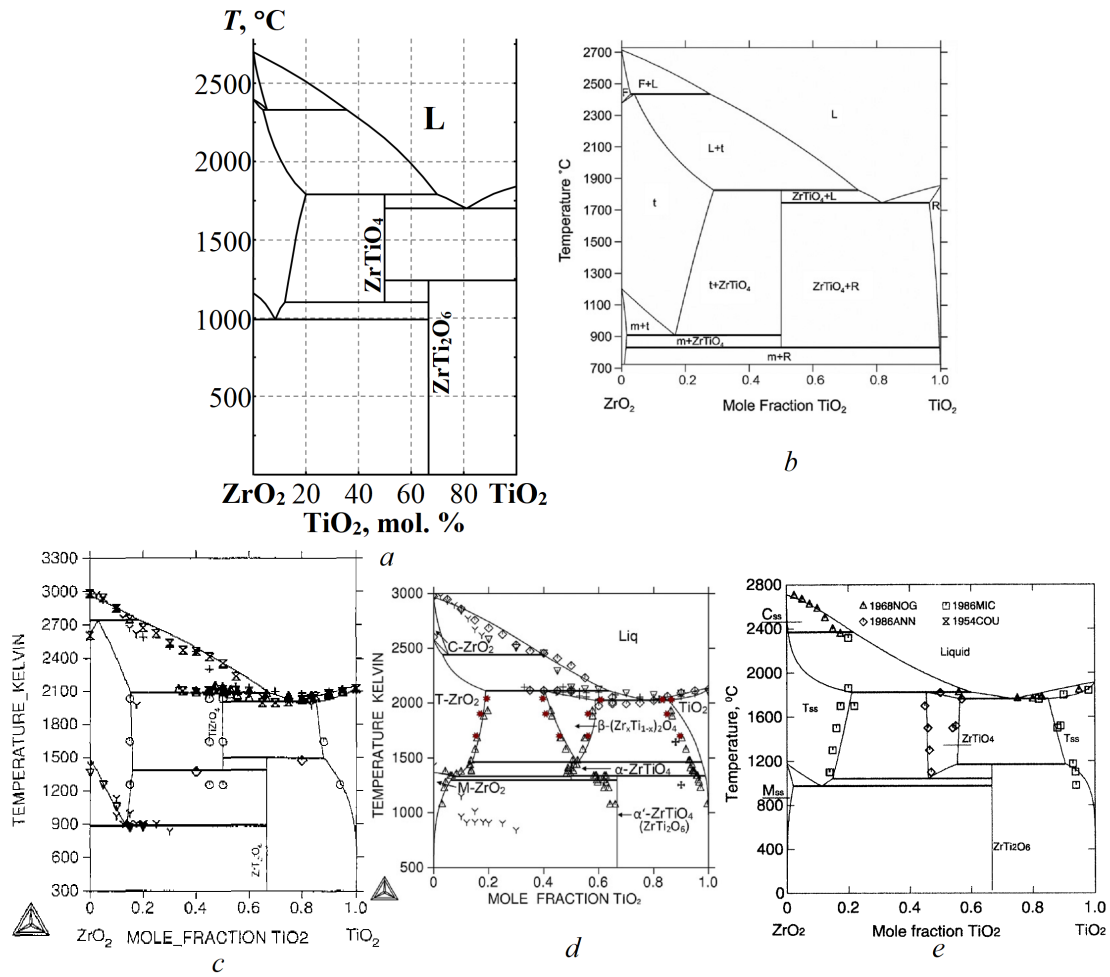
FIG. 5. Phase diagram of the TiO$_2$–ZrO$_2$ system (thermodynamic optimization): *a* – [85, 87], *b* – [97], *c* – [91], *d* – [98], *e* – [90]; ss – solid solution, *m*-, *t*-, *c*- – monoclinic, tetragonal and cubic polymorph, respectively, R – rutile, L – liquid

Fig. 5*a* shows a calculated version of the phase diagram based on data from [87]. The diagram was calculated using the known thermodynamic data for ZrO$_2$, various estimates for TiO$_2$ based on correlations between the interaction parameters and ionic radius [85], and other data. To model the mixing of components, a simple subregular model was adopted using only the ideal entropy of mixing and without taking into account any temperature dependence of the mixing parameter coefficients. The thermodynamic properties of the ZrTiO$_4$ and ZrTi$_2$O$_6$ compounds relative to hypothetical "cubic" TiO$_2$ have been determined to comply with the published experimental phase relationships.

Various interaction parameters were used for the crystalline and liquid phases, the solubility of ZrO$_2$ in TiO$_2$ was neglected. The parameter of interaction of the liquid phase was adjusted in such a way as to reproduce the peritectic melting of ZrTiO$_4$ at 1820 °C, as well as a temperature of 1760 °C and a composition of 80 mol. % TiO$_2$ corresponding to the eutectic point.

The thermodynamic optimization of the TiO$_2$–ZrO$_2$ phase diagram performed in [97] are in good agreement with the available experimental data (Fig. 5*b*). The presence of two-phase fields between pyrochlore and ZrTiO$_4$, as well as between pyrochlore and *t*-ZrO$_2$ at 1300 °C, which were not considered in earlier versions of the phase diagram, is essential. Two invariant transition-type reactions were found in calculations and then experimentally confirmed in the temperature range between 1300 and 1500 °C.

The phase diagram of the TiO$_2$–ZrO$_2$ system, calculated on the basis of the available experimental data [70–72, 74–76, 79, 83], based on the fact that ZrTiO$_4$ and ZrTi$_2$O$_6$ are taken as peritectically decomposing stoichiometric compounds, is shown in Fig. 5*c* according to the data of [91].

The phase diagram and thermodynamic data available for the TiO$_2$–ZrO$_2$ system were reviewed. An attempt was made to provide a consistent set of thermodynamic parameters describing the system by combining the CALPHAD

method using Thermo-Calc software and a database system. The set of thermodynamic functions is intended for a simplified version of the TiO$_2$–ZrO$_2$ phase diagram, in which ZrTiO$_4$ and ZrTi$_2$O$_6$ are considered as stoichiometric compounds. Comprehensive comparisons are made with the available experimental data, and it is shown that the set can satisfactorily take into account most of the experimental data, with the exception of the data on the homogeneity of ZrTiO$_4$ and ZrTi$_2$O$_6$.

The thermodynamically optimized phase diagram of the TiO$_2$–ZrO$_2$ system according to experimental data [98] and data from other authors is shown in Fig. 5*d*.

The phase relationships in the TiO$_2$–ZrO$_2$ system were studied in the temperature range from 1000 to 1600 °C using X-ray diffractometry and scanning electron microscopy (SEM) with energy dispersive X-ray spectrometry (EDS). The temperature of peritectic reactions Liquid = β-(Zr$_x$Ti$_{1-x}$)$_2$O$_4$ + TiO$_2$ and Liquid + t-ZrO$_2$ = β-(Zr$_x$Ti$_{1-x}$)$_2$O$_4$ were determined to be 1756 and 1844 °C, respectively.

The compositions of the eutectic were determined by SEM/EDS as 83.2 ± 1.0 mol. % TiO$_2$. The temperature of the eutectic reaction Liquid = β-(Zr$_x$Ti$_{1-x}$)$_2$O$_4$ + TiO$_2$ determined in this work is in good agreement with other data. The eutectic composition measured in this work contains more TiO$_2$ compared to previous results. However, the results obtained are within the uncertainty of experimental methods. The enthalpy of formation of the β-ZrTiO$_4$ compound from oxides was measured to be –18.3 ± 5.3 kJ/mol using capillary calorimetry.

The molar heat capacities of the β-(Zr$_x$Ti$_{1-x}$)$_2$O$_4$ compound were measured in the range –38–950 °C. Experimental data were used for the thermodynamic values (i.e., the heat capacity and enthalpy of formation of the β-ZrTiO$_4$ compound) measured in this work. In order to optimize the description of the heat capacity of α-ZrTiO$_4$ and β-(Zr$_x$Ti$_{1-x}$)$_2$O$_4$, as well as the contribution of the enthalpy of formation of the β-Zr$_x$Ti$_{1-x}$O$_4$ phase, respectively. Using the obtained experimental results together with the literature data, thermodynamic parameters were obtained in the TiO$_2$–ZrO$_2$ system.

In [90], a thermodynamic description of the TiO$_2$–ZrO$_2$ system based on a critical evaluation of limited experimental data from literature is obtained. Non-stoichiometric compound ZrTiO$_4$ is described as (Ti,Zr)$_1$O$_2$ while ZrTi$_2$O$_6$ is treated as a stoichiometric phase. Comparison shows that the calculated phase diagram agrees reasonably with the experimental set selected by authors (Fig. 5*e*).

So, in this system, there are many contradictions in both experimental and calculated data. In general, we can conclude that this system needs detailed revision, with independent experimental and calculation expertise.

4. SiO$_2$–ZrO$_2$ system

Interest in the phase relationships in the SiO$_2$–ZrO$_2$ system in connection with the need for these data for the technology of baddeleyite and zircon refractories has not weakened since [108]. The known variants of state diagrams are shown in Fig. 6.

The most complete version is presented in the experimental work [109] (Fig. 6*b*). Subsequent works are only clarifying on the temperature boundaries of the existence of zircon [110] (Fig. 6*b*), on the region of solid solutions [111] (Fig. 6*c*), and on the border of metastable miscibility gap and the critical point of the immiscible region [112] (Fig. 6*c*).

In [113] (Fig. 6*d*), the Gibbs energies of three solid polymorphic and liquid ZrO$_2$ were again optimized based on a critical assessment of all available experimental data. All data from the experimental phase diagram and thermodynamic properties of the solid and liquid phases in each binary system were simultaneously evaluated and optimized to obtain a set of model parameters. Certain discrepancies in the phase diagram and thermodynamic data in the literature were eliminated with this optimization. Any type of thermodynamic data and phase equilibria can be calculated using models with optimized parameters.

It can be concluded that this system has been studied in sufficient detail and no additional research is required on it. However, if we discuss the nanoscale state of the components of this system, then it is possible for the manifestation of features that appear to contradict the available data on phase equilibria, for example, the phenomenon of phase selection [114].

An example of phase selection, which is a consequence of the fact that for the formation of a critical nucleus, the condition of a minimum distance between nanoparticles of more than half the size of the critical nucleus must be met, can be the nature of the course of solid-phase processes in systems with different reagent particle sizes of. In particular, the study of the interaction between ZrO$_2$ and SiO$_2$ showed that the use of a mixture of ZrO$_2$ nanoparticles (15–20 nm) with amorphous SiO$_2$ nanoparticles (about 5 nm) as a reaction composition does not lead to the formation of ZrSiO$_4$, but crystallization of cristobalite occurs. At the same time, during thermal treatment of a mixture of ZrO$_2$ particles tens of micrometers in size with the same SiO$_2$ nanoparticles, ZrSiO$_4$ is formed in significant amounts. The explanation for this phenomenon, unusual for the kinetics of solid-phase reactions, when a decrease in the particle size of reagents causes a decrease in the rate of the chemical reaction, is that the size of the critical ZrSiO$_4$ nucleus is much
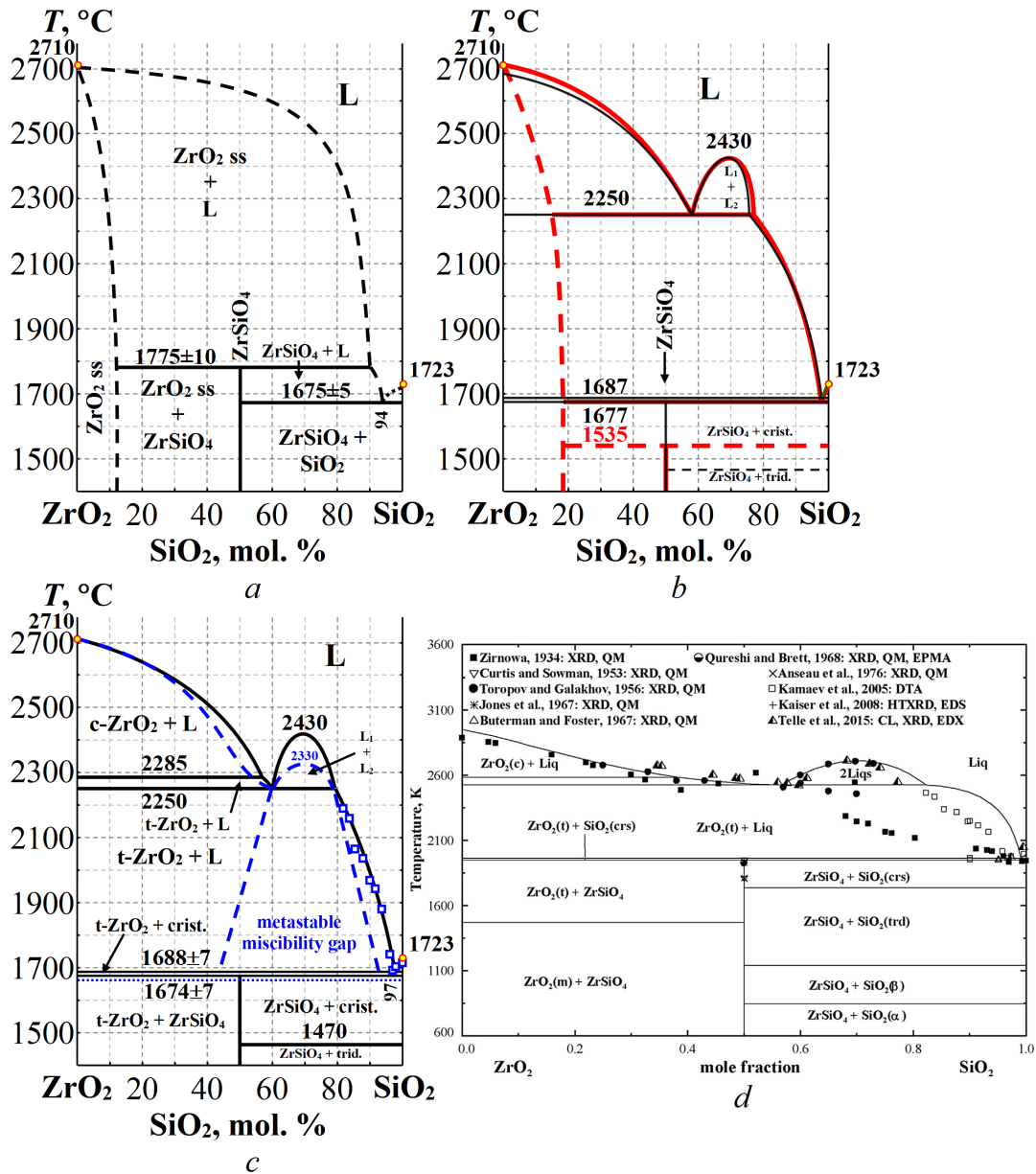
FIG. 6. Phase diagram of the SiO₂–ZrO₂ system: *a* – [108]; *b* – red line [109], black line [110]; *c* – black line [111], blue line and dots [112], *d* – [113]; ss – solid solution, *m*-, *t*-, *c* – monoclinic, tetragonal and cubic polymorph, respectively, trid. – tridymite, crist. – cristobalite, L – liquid

larger than the distance between ZrO₂ nanoparticles in the reaction composition of ZrO₂ and SiO₂ nanoparticles [114]. At the same time, crystallization of cristobalite in a composition of ZrO₂ and SiO₂ nanoparticles is possible, which is explained by the small size of the nuclei of this phase.

It should also be noted that isostructural ZrSiO₄ uranium silicate is not formed by high-temperature methods, but is easily synthesized under hydrothermal conditions at relatively low temperatures [115].

5. TiO₂–SiO₂–ZrO₂ system

There are only a few brief works on the study of the TiO₂–SiO₂–ZrO₂ ternary system [51, 116, 117]. In [116], a projection of the liquidus surface was constructed, on which the dashed line indicates the immiscibility area (Fig. 7*a*), as well as two isothermal sections at 1400 °C (Fig. 7*b*) and at 1500 °C (Fig. 7*c*).
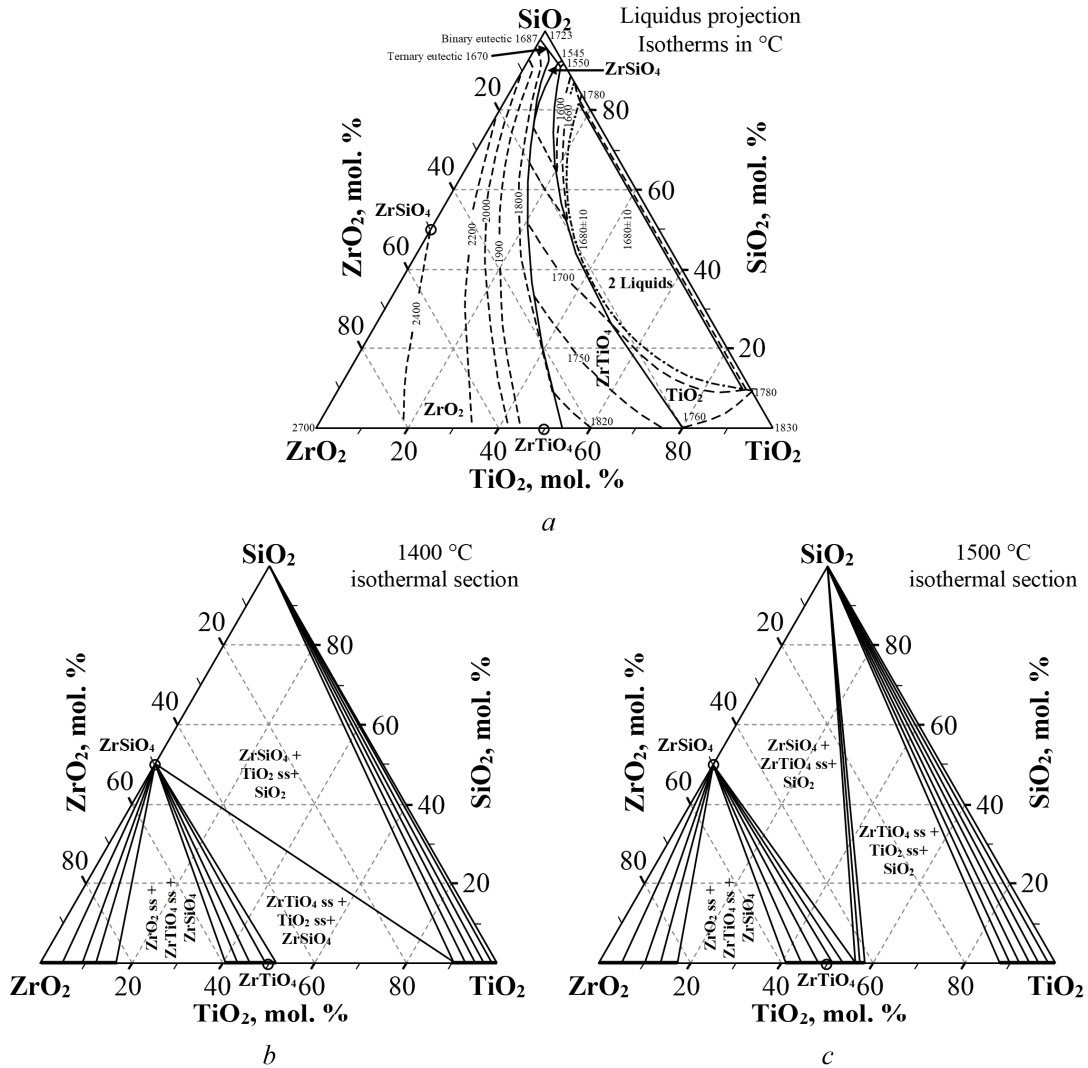
FIG. 7. Phase diagram of the TiO$_2$–SiO$_2$–ZrO$_2$ system [116]: *a* – liquidus surface projection; *b* – 1400 °C isothermal section; *c* – 1500 °C isothermal section, ss – solid solution

Initial reagents are not described. The original compositions were taken according to previous studies [51, 117] to clarify the critical points. The exact compositions are not given, as are the instruments or research methods. However, most likely, the DTA method was used to obtain data of this type in this temperature range.

Fig. 7*a* is taken from [51] with modification according to the results of study [116] (Fig. 7*b,c*) present a summary of several experimental studies of the ZrSiO$_4$–TiO$_2$ system [117] and the TiO$_2$–ZrO$_2$ system [70]. Data are summarized as preliminary experimental results. Three peritectics and one eutectic were found. Only a eutectic at 1500 °C has been suggested by earlier studies in this system. The new critical points appear to be consistent with experimental observations of the cooling and crystallization behavior of the respective compositions, as shown in Fig. 7. Thus, the system needs further detailed research.

6. Conclusions

The incompleteness, contradictions of the available data and the arising problems in the interpretation of study results are demonstrated. As an example, the proposed in [116] topology of the liquidus surface in ternary system does not take into account the presence of a miscibility gap in the binary section of the SiO$_2$–ZrO$_2$ system, as well as the character of the liquidus line in the binary TiO$_2$–ZrO$_2$ system.

It should be noted that during the preparation of this review a perfect tool was actively used to search for information on phase diagrams – Phase Equilibria Diagrams Online Search System by NIST ACerS [118], which unfortunately has limited availability for free use. The development of such tools and databases makes it possible to significantly

simplify the search for the necessary information [119] and reduce routine procedures to a possible minimum [120]. It would be beneficial to see more of these tools, not only commercial, but also freely available. This will undoubtedly contribute to progress in materials science and technology.

The analyzed information allows us to conclude that the design of new materials based on the TiO_2–SiO_2–ZrO_2 system with a given set of physicochemical, structural and dimensional parameters without using data on phase equilibria is almost impossible. It should be especially emphasized that the greatest contradictions in the data are observed in the synthesis and analysis of nanoscale substances and nanomaterials. This feature of the nanoscale state leads to the conclusion that, for completeness, it is necessary to add a dimension factor to the analysis of phase equilibria. At the same time, there are still few examples of such an approach [106]. This greatly complicates and constrains the possibilities of directed synthesis and analysis of nanoscale objects. Thus, a wide field for experiments opens in front of us – a new dimension and a new life of classical physicochemical analysis. By combining the acquisition of these data with the development of software tools that make it possible to work with them comfortably and efficiently, it is possible to bring the design of nanoscale substances and nanostructured materials to a brand-new level.

The question is in which field the new approach will be firstly applied. Of course, for a precedent to grab the attention of researchers, it must be a critically important task in a topical area.

Of great concern today is the energy crisis and the ways out of it. The emphasis is shifting towards nuclear energy as the main hope of overcoming energy and resource problems. But the fact is that at the dawn of the century of atomic energy a great leap forward was made. Many options have been tried, out of which a small number of solutions were preferred. At that date and level of knowledge these decisions seemed optimal. But, the experience of nuclear power development has shown that there are serious safety problems for the most popular solution which seemed ideal – for oxide nuclear fuel in a zirconium cladding.

The serious problem is the zirconium reaction with vapor. If this reaction occurs, then it launches a chain of negative events that aggravate each other. As a result, the probability is very high that a nuclear power plant have a severe accident, such as the Chernobyl and Fukushima-1 accidents, could occur. Thus, with the renaissance of nuclear energy for preventing the described problem, began the development new safer options for fuel assemblies – an advanced accident-tolerant fuel.

One of the solutions to improve fuel safety is the use of special coatings to protect the cladding from oxidation. In particular, a promising coating option are MAX-phases, that have a good compatibility with the cladding material, high ductility and, potentially, good resistance to high temperatures.

At the same time, these phases and their combinations with metallic and oxide materials have not practically been studied, and we need experimental and theoretical evidence of their effectiveness. The first and most important step on the way is the study of phase equilibria. In particular, it is necessary to know what happens with that coating under oxidizing conditions at high temperatures. This requires comprehensive physicochemical information not only about MAX-phases, but their oxidation products and possible interactions.

For that, a critical analysis was carried out for the synthetic possibilities, the conditions for high-temperature experiments, the assessment of nonequilibrium phase formation in binary systems and information about the TiO_2–SiO_2–ZrO_2 system which is the currently available. It will allow us to further take into account the features of phase formation and phase equilibria in the TiO_2–SiO_2–ZrO_2 system at high temperatures and in nanoscale to evaluate the stability limits of MAX-phases in conditions at severe accidents on nuclear power plants.

Successful implementation of this or another actual problem must demonstrate the effectiveness of the described approach. We are hope to see this.

Acknowledgement

References

[1] Retention of Molten Core Materials in Water-Cooled Reactors (RASPLAV and MASCA International Projects), Ed. by V.G. Asmolov, A.Yu. Rumyantsev, and V.F. Strizhov, Moscow, Rosenergoatom, 2018, 576 p. [in Russian].

[2] Gonzalez-Julian J. Processing of MAX phases: From synthesis to applications. *J. Am. Ceram. Soc.*, 2021, **104**(2), P. 659–690.

[3] Zhang Z., Duan X., Jia D., Zhou Y., van der Zwaag S. On the formation mechanisms and properties of MAX phases: A review. *J. Eur. Ceram. Soc.*, 2021, **41**(7), P. 3851–3878.

[4] Medvedeva N.I., Enyashin A.N., Ivanovskii A.L. Modeling of the electronic structure, chemical bonding, and properties of ternary silicon carbide Ti_3SiC_2. *J. Struct. Chem.*, 2011, **52**(4), P. 785–802.

[5] Arkundato A., Hasan M., Pramutadi A., Rivai A.K., Su'ud Z. Thermodynamics and Structural Properties of Ti$_3$SiC$_2$ in Liquid Lead Coolant. *J. Phys. Conf. Ser.*, 2020, **1493**, Article 012026.

[6] Tretyakov Yu.D. Self-organisation processes in the chemistry of materials. *Russ. Chem. Rev.*, 2003, **72**(8), P. 651–679.

[7] Gleiter H. Nanostructured materials: Basic concepts and microstructure. *Acta Mater.*, 2000, **48**(1), P. 1–29.

[8] Ozin G.A., Arsenault A.C., Cademartiri L. *Nanochemistry: A Chemical Approach to Nanomaterials*, 2nd ed. Cambridge: Royal Society of Chemistry, 2009, 820 p.

[9] Ivanov V.V., Talanov V.M. Principle of modular building of nanostructures: the information codes and the combinatorial design. *Nanosyst.: Phys. Chem. Math.*, 2010, **1**(1), P. 72–107 [in Russian].

[10] Galakhov F.Ya., Varshal B.G. On the causes of liquation in simple silicate systems. Proceedings of the First All-Union Symposium "Liquidation Phenomena in Glass", Leningrad, April 16–18, 1968, Leningrad: "Nauka", 1969, P. 6–11 [in Russian].

[11] Porai-Koshits E.A., Averyanov V.I. On the phenomena of primary and secondary immiscibility in glasses. Proceedings of the First All-Union Symposium "Liquidation Phenomena in Glass", Leningrad, April 16–18, 1968, Leningrad, Nauka, 1969, P. 26–30 [in Russian].

[12] Galakhov F.Ya. Microliquation and Its Image on the Binary System State Diagram. *Bull. Acad. Sci. USSR, Chem. Ser.*, 1964, **8**, P. 1377–1383 [in Russian].

[13] Andreev N.S., Mazurin O.V., Porai-Koshits E.A., Roslova G.P., Filippovich V.N. *Phenomena of liquation in glasses*. Ed. M.M. Schultz, Leningrad, Nauka, 1974, 217 p. [in Russian].

[14] Hudon P., Baker D.R. The nature of phase separation in binary oxide melts and glasses. I. Silicate systems. *J. Non-Cryst. Solids*, 2002, **303**(3), P. 299–345.

[15] Hudon P., Baker D.R. The nature of phase separation in binary oxide melts and glasses. II. Selective solution mechanism. *J. Non-Cryst. Solids*, 2002, **303**(3), P. 346–353.

[16] Hudon P., Baker D.R. The nature of phase separation in binary oxide melts and glasses. III. Borate and germanate systems. *J. Non-Cryst. Solids*, 2002, **303**(3), P. 354–371.

[17] Mriglod I.M., Patsagan O.V., Melnik R.S. Metastable liquation processes in multicomponent glass-forming systems: a review of experimental and theoretical results; phase diagrams with metastable segregation. Preprint IFCS NAS Ukraine, ICMP-03-15U, 2003, 22 p. [In Ukrainian].

[18] Kündig A.A., Ohnuma M., Ping D.H., Ohkubo T., Hono K. In situ formed two-phase metallic glass with surface fractal microstructure. *Acta Mater.*, 2004, **52**(8), P. 2441–2448.

[19] Chang H.J., Yook W., Park E.S., Kyeong J.S., Kim D.H. Synthesis of metallic glass composites using phase separation phenomena. *Acta Mater.*, 2010, **58**(7), P. 2483–2491.

[20] Delitsyn L.M. Liquid immiscibility phenomena in magmatic systems, Moscow, GEOS, 2010, 222 p.

[21] Blinova I.V., Gusarov V.V., Popov I.Yu. "Almost quasistationary" approximation for the problem of solidification front stability. *Z. Angew. Math. Phys.*, 2009, **60**(1), P. 178–188.

[22] Eliseev A.A., Lukashin A.V. Functional nanomaterials. Ed. Yu.D. Tretyakov. Moscow, FIZMATLIT, 2010, 456 p.

[23] Trusov L.A., Zaitsev D.D., Kazin P.E., Tret'yakov Yu.D., Jansen M. Preparation of Magnetic Composites through SrO–Fe$_2$O$_3$–Al$_2$O$_3$–B$_2$O$_3$ Glass Crystallization. *Inorg. Mater.*, 2009, **45**(6), P. 689–693.

[24] Kazin P.E., Trusov L.A., Zaitsev D.D., Tret'yakov Yu.D. Glass Crystallization Synthesis of Ultrafine Hexagonal M-Type Ferrites: Particle Morphology and Magnetic Characteristics. *Russ. J. Inorg. Chem.*, 2009, **54**(14), P. 2081–2090.

[25] Kazin P.E., Trusov L.A., Kushnir S.E., Yaroshinskaya N.V., Petrov N.A., Jansen M. Hexaferrite Submicron and Nanoparticles with Variable Size and Shape via Glass-Ceramic Route. *J. Phys. Conf. Ser.*, 2010, **200**(7), Article 072048.

[26] Khodakovskaya R.Ya. Chemistry of titanium-containing glasses and sitalls. Moscow, Khimiya, 1978, 288 p. [in Russian].

[27] von Olleschik-Elbheim L., el Baya A., Schmidt M.A., Zhu D.-M., Kosugi T. Thermal conductivity of GeO$_2$–SiO$_2$ and TiO$_2$–SiO$_2$ mixed glasses. *J. Non-Cryst. Solids*, 1996, **202**(1), P. 88–92.

[28] You H., Nogami M. Persistent spectral hole burning of Eu^{3+} ions in TiO$_2$–SiO$_2$ glass prepared by sol-gel method. *J. Alloys Compd.*, 2006, **408–412**, P. 796–799.

[29] Lebedeva G.A. Formation of a liquation structure in titanium-containing aluminosilicate glasses. *Glass and Ceramics*, 2008, **9**, P. 25–28 [in Russian].

[30] Scannell G., Koike A., Huang L. Structure and thermo-mechanical response of TiO$_2$–SiO$_2$ glasses to temperature. *J. Non-Cryst. Solids*, 2016, **447**, P. 238–247.

[31] Romy Dwipa Y. Away, Chika Takai-Yamashita, Takayuki Ban, Yutaka Ohya. Photocatalytic properties of TiO$_2$–SiO$_2$ sandwich multilayer films prepared by sol-gel dip-coating. *Thin Solid Films*, 2021, **720**, Article 138522.

[32] Yorov K.E., Kolesnik I.V., Romanova I.P., Mamaeva Yu.B., Lermontov S.A., Kopitsa G.P., Baranchikov A.E., Ivanov V.K. Engineering SiO$_2$–TiO$_2$ binary aerogels for sun protection and cosmetic applications. *J. Supercrit. Fluid.*, 2021, **169**, Article 105099.

[33] Sun S., Ding H., Wang J., Li W., Hao Q. Preparation of a microsphere SiO$_2$/TiO$_2$ composite pigment: The mechanism of improving pigment properties by SiO$_2$. *Ceram. Int.*, 2020, **46**(14), P. 22944–22953.

[34] Llamas S., Ponce Torres A., Liggieri L., Santini E., Ravera F. Surface properties of binary TiO$_2$–SiO$_2$ nanoparticle dispersions relevant for foams stabilization. *Colloids Surf. A Physicochem. Eng. Asp.*, 2019, **575**, P. 299–309.

[35] Ren Y., Li W., Cao Z., Jiao Y., Xu J., Liu P., Li S., Li X. Robust TiO$_2$ nanorods-SiO$_2$ core-shell coating with high-performance self-cleaning properties under visible light. *Appl. Surf. Sci.*, 2020, **509**, Article 145377.

[36] Wang T., Li Y., Wu W.-T., Zhang Y., Wu L., Chen H. Effect of chiral-arrangement on the solar adsorption of black TiO$_2$–SiO$_2$ mesoporous materials for photodegradation and photolysis. *Appl. Surf. Sci.*, 2021, **537**, Article 148025.

[37] Bao Y., Guo R., Gao M., Kang Q., Ma J. Morphology control of 3D hierarchical urchin-like hollow SiO$_2$@TiO$_2$ spheres for photocatalytic degradation: Influence of calcination temperature. *J. Alloys Compd.*, 2021, **853**, Article 157202.

[38] Shabanova N.A., Popov V.V., Sarkisov P.D. *Chemistry and technology of nanodispersed oxides*. Moscow, Akademkniga, 2006, 309 p. [in Russian].

[39] Ermilov P.I., Indeikin E.A., Tolmachev I.A. Pigments and pigmented paintwork materials. Leningrad, Khimiya, 1987, 200 p. [in Russian].

[40] *Titanium Dioxide (TiO$_2$) and Its Applications*. A volume in Metal Oxides. Edited by F. Parrino, L. Palmisano. Amsterdam, Elsevier, 2020, 702 p.

[41] Rieke R. Melting Influence of Titanic Acid on Silica, Alumina, and Kaolin. *Sprechsaal*, 1908, **41**, P. 405.

[42] Umezu S., Kakiuchi F. Investigations on Iron Blast. Furnace Slags Containing Titanium. *Nippon Kogyo Kwaishi*, 1930, **46**, P. 866–877.

[43] Bogatzkii D.P. Investigation of the system TiO_2–SiO_2. *Metallurgist*, 1938, **11**, P. 59–67 [in Russian].

[44] Bunting E.N. Phase equilibria in the systems. TiO_2, TiO_2–SiO_2, and TiO_2–Al_2O_3. *J. Res. Nat. Bur. Stand.*, 1933, **11**(5), P. 719–725.

[45] Ricker R.W., Hummel F.A. Reactions in the System TiO_2–SiO_2; Revision of the Phase Diagram. *J. Amer. Ceram. Soc.*, 1951, **34**(9), P. 271–279.

[46] DeVries R.C., Roy R., Osborn E.F. The System TiO_2–SiO_2. *Trans. Brit. Ceram. Soc.*, 1954, **53**(9), P. 525–540.

[47] Kaufman L. Calculation of multicomponent ceramic phase diagrams. *Physica B+C (Amsterdam)*, 1988, **150**(1–2), P. 99–114.

[48] Kubaschewski O., Alcock C.B. International Series on Materials Science and Technology, V. 24 (Metallurgical Thermochemistry), 5th ed. Oxford, United Kingdom: Pergamon Press, Elsevier Science Ltd., 1979, 449 p.

[49] DeCapitani C., Kirschen M. A generalized multicomponent excess function with application to immiscible liquids in the system CaO–SiO_2–TiO_2. *Geochim. Et Cosmochim. Acta*, 1998, **62**(23/24), P. 3753–3763.

[50] Kirschen M., DeCapitani C., Millot F., Rifflet J.-C., Coutures J.-P. Immiscible silicate liquids in the system SiO_2–TiO_2–Al_2O_3. *Eur. J. Mineral.*, 1999, **11**, P. 427–440.

[51] Don McTaggart G., Andrews A.I. Immiscibility Area in the System TiO_2–ZrO_2–SiO_2. *J. Am. Ceram. Soc.*, 1957, **40**(5), P. 167–170.

[52] Massazza F., Sirchia E. Il sistema MgO–SiO_2–TiO_2. *La Chimica e l'industria*, 1958, **XL**(5), P. 376–380.

[53] Galakhov F.Ya., Areshev M.P., Vavilonova V.T., Aver'yanov V.I. Determination of the boundaries of metastable liquation in the silica part of the TiO_2–SiO_2 system. *Izv. Akad. Nauk SSSR, Ser. Neorg. Mater.*, 1974, **10**(1), P. 179–180 [in Russian].

[54] Saunders N., Miodownik A.P. CALPHAD (calculation of phase diagrams): a comprehensive guide. Pergamon materials series. Vol. 1, 1998, 479 p.

[55] Kamaev D.N. High-temperature phase equilibria in TiO_2–SiO_2, ZrO_2–Al_2O_3, ZrO_2–SiO_2, FeO–ZrO_2–SiO_2, Fe–Zr–Si–O systems: dissertation ... candidate of chemical sciences: 02.00.04. Chelyabinsk, 2005, 168 p. [in Russian].

[56] Mikhailov G.G., Novolotskiy D.Ya. Thermodynamics of steel deoxidation. Moscow, Metallurgy, 1993, 114 p. [in Russian].

[57] Kirillova S.A., Al'myashev V.I., Gusarov V.V. Phase Relationships in the SiO_2–TiO_2 System. *Russ. J. Inorg. Chem.*, 2011, **56**(9), P. 1464–1471.

[58] Kirillova S.A., Almjashev V.I., Gusarov V.V. Spinodal decomposition in the SiO_2–TiO_2 system and hierarchically organized nanostructures formation. *Nanosyst.: Phys. Chem. Math.*, 2012, **3**(2), P. 100–115 [in Russian].

[59] Gurvich L.V., Iorish V.S., Chekhovskoi D.V., Yungman V.S. IVTANTHERMO – A Thermodynamical Database and Software System for the Personal Computer. User's Guide. CRC Press, Inc., Boca Raton, 1993.

[60] Hlaváč J. Melting temperatures of refractory oxides: Part I. *Pure & Appl. Chem.*, 1982, **54**(3), P. 681–688.

[61] Chase Jr., M.W. NIST-JANAF Thermochemical Tables (Journal of Physical and Chemical Reference Data Monographs), 4th ed., Monograph No. 9. American Institute of Physics, 1998–2000, 1952 p.

[62] Almjashev V.I., Gusarov V.V., Khabensky V.B., Bechta S.V., Granovsky V.S. Influence of the temperature difference at immiscibility liquids interface on their phase instability. OECD/NEA MASCA2 Seminar 2007, Cadarache, France, 11–12 October 2007, 2007, paper 3.3.

[63] Boulay E., Nakano J., Turner S., Idrissi H., Schryvers D., Godet S. Critical assessments and thermodynamic modeling of BaO–SiO_2 and SiO_2–TiO_2 systems and their extensions into liquid immiscibility in the BaO–SiO_2–TiO_2 system. *CALPHAD*, 2014, **47**, P. 68–82.

[64] Lu X., Jin Z. Thermodynamic assessment of the BaO–TiO_2 quasibinary system. *CALPHAD*, 2000, **24**(3), P. 319–338.

[65] Stolyarova V.L., Lopatin S.I. Mass-spectrometric study of the vaporization and thermodynamic properties of components in the BaO–TiO_2–SiO_2 system. *Glass Phys. Chem.*, 2005, **31**(2), P. 132–137.

[66] Zhang C., Ge X., Hu Q., Yang F., Lai P., Shi C., Lu W., Li J. Atomic scale structural analysis of liquid immiscibility in binary silicate melt: A case of SiO_2–TiO_2 system. *J. Mater. Sci. Technol.*, 2020, **53**, P. 53–60.

[67] Von Wartenberg H., Gurr W. Schmelzdiagramme höchstfeuerfester Oxyde. III. *Z. Anorg. Allg. Chem.*, 1931, **196**(1), P. 374–383.

[68] Büssem W., Schusterius C., Ungewiss A. X-Ray Investigations of the Binary Systems TiO_2–MgO, ZrO_2–MgO, and ZrO_2–TiO_2. *Ber. Dtsch. Keram. Ges.*, 1937, **18**(10), P. 433–443.

[69] Sowman H.G., Andrews A.I. A Study of the Phase Relations of ZrO_2–TiO_2 and ZrO_2–TiO_2–SiO_2. *J. Am. Ceram. Soc.*, 1951, **34**(10), P. 298–301.

[70] Coughanour L.W., Roth R.S., DeProsse V.A. Phase equilibrium relations in the systems lime-titania and zirconia-titania. *J. Res. Natl. Bur. Stand. (U. S.)*, 1954, **52**(1), P. 37–42.

[71] Brown Jr. F.H., Duwez P. The Zirconia-Titania System. *J. Am. Ceram. Soc.*, 1954, **37**(3), P. 129–132.

[72] Cocco A., Torriano G. Relations between the solid phases in the system ZrO_2–TiO_2. *Ann. Chim. (Rome)*, 1965, **55**(3), P. 153–163.

[73] Cocco A., Torriano G. *Ann. Chim. (Rome)*, 1958, **48**(8/9), P. 587–599.

[74] Webster A.H., MacDonald R.C., Bowman W.S. The System PbO–ZrO_2–TiO_2 at 1100 °C. *J. Can. Ceram. Soc.*, 1965, **34**, P. 97–102.

[75] Noguchi T., Mizuno M. Phase changes in solids measured in a solar furnace ZrO_2–TiO_2 system. *Sol. Energy*, 1967, **11**(1), P. 56–61.

[76] Noguchi T., Mizuno M. Phase changes in the ZrO_2–TiO_2 system. *Bull. Chem. Soc. Jpn.*, 1968, **41**(12), P. 2895–2899.

[77] Sugai T., Hasegawa S. Growth of zirconium titanate ($ZrTiO_4$) single crystals from molten salts. *J. Geram. Assoc. Japan*, 1968, **76**(12), P. 429–430.

[78] Ono A. Solid solutions in the system ZrO_2–TiO_2. *Mineral. J.*, 1972, **6**(6), P. 433–441.

[79] Shevchenko A.V., Lopato L.M., Maister I.M., Gorbunov O.S. The TiO_2–ZrO_2 system. *Russ. J. Inorg. Chem.*, 1980, **25**(9), P. 1379–1381.

[80] Willgallis A., Seigmann E., Hettiarachi T. Srilankite, a new Zr-Ti-oxide mineral. *Neues Jahrb. für Mineral. Monatshefte*, 1983, **4**, P. 151–157.

[81] Domingues L.P., McHale A.E., Negas T., Roth R.S. Processing and properties of $ZrTiO_4$-Based Ceramics; P. A21-A21 in International Conf. on the Science and Technology of Zirconia, Extended Abstract, 2nd, Stuttgart, Germany, June 21–23, 1983.

[82] McHale A.E., Roth R.S. Investigation of the Phase Transition in $ZrTiO_4$ and $ZrTiO_4$-SnO_2 Solid Solutions. *J. Am. Ceram. Soc.*, 1983, **66**(2), P. C18–C20.

[83] McHale A.E., Roth R.S. Low-Temperature Phase Relationships in the System ZrO_2–TiO_2. *J. Am. Ceram. Soc.*, 1986, **69**(11), P. 827–832.

[84] Bordet P., McHale A.E., Santoro A., Roth R.S. Powder neutron diffraction study of $ZrTiO_4$, $Zr_5Ti_7O_{24}$, and $FeNb_2O_6$. *J. Solid State Chem.*, 1986, **64**(1), P. 30–46.

[85] Kim D.-J. Lattice Parameters, Ionic Conductivities, and Solubility Limits in Fluorite-Structure MO_2 Oxide [$M = Hf^{4+}$, Zr^{4+}, Ce^{4+}, Th^{4+}, U^{4+}] Solid Solutions. *J. Am. Ceram. Soc.*, 1989, **72**(8), P. 1415–1421.

[86] Christoffersen R., Davies P.K. Structure of Commensurate and Incommensurate Ordered Phases in the System ZrTiO$_4$–Zr$_5$Ti$_7$O$_{24}$. *J. Am. Ceram. Soc.*, 1992, **75**(3), P. 563–569.

[87] Yokokawa H., Sakai N., Kawada T., Dokiya M. Phase Diagram Calculations for ZrO$_2$ Based Ceramics: Thermodynamic Regularities in Zirconate Formation and Solubilities of Transition Metal Oxides. P. 59–68 in Sci. Technol. Zirconia V, [Int. Conf.], 5th, Melbourne, Australia, August 16–21, 1992. Edited by S.P.S. Badwal, M.J. Bannister, and R.H.J. Hannink, Technomic Publishing Co., Inc., Lancaster, Pennsylvania, 1993.

[88] Kobayashi K., Kato K., Terabe K., Yamaguchi S., Iguchi Y. Metastable Phase Relationship in the ZrO$_2$–YO$_{1.5}$, ZrO$_2$–TiO$_2$ and YO$_{1.5}$–TiO$_2$ Systems. *J. Ceram. Soc. JAPAN*, 1998, **106**(1236), P. 782–786.

[89] Sham E.L., Aranda M.A.G., Farfan-Torres E.M., Gottifredi J.C., Martínez-Lara M., Bruque S. Zirconium titanate from sol–gel synthesis: thermal decomposition and quantitative phase analysis. *J. Solid State Chem.*, 1998, **139**(2), P. 225–232.

[90] Gong W., Jin Z., Du Y. Thermodynamic Assessment of the ZrO$_2$–TiO$_2$ Quasibinary System. *J. Min. Met.*, 2000, **36**(3–4)B, P. 123–132.

[91] Park J.-H., Liang P., Seifert H.J., Aldinger F., Koo B.-K., Kim H.-G. Thermodynamic Assessment of the ZrO$_2$–TiO$_2$ System. *J. Korean Ceram. Soc.*, 2001, **7**(1), P. 11–15.

[92] Troitzsch U., Ellis D.J. High-PT study of solid solutions in the system ZrO$_2$-TiO$_2$: The stability of srilankite. *Eur. J. Mineral.*, 2004, **16**(4), P. 577–584.

[93] Troitzsch U., Christy A.G., Ellis D.J. Synthesis of Ordered Zirconium Titanate (Zr,Ti)$_2$O$_4$ from the Oxides Using Fluxes. *J. Am. Ceram. Soc.*, 2004, **87**(11), P. 2058–2063.

[94] Troitzsch U., Ellis D.J., Christy, A.G. (2003–2006). Patent: Synthesis of Ceramic Crystals. Patent Application No. 2003906410 (Australian), PCT/AU2004/001615 WO 2005049497 (International).

[95] Troitzsch U., Christy A.G., Ellis D.J. The crystal structure of disordered (Zr,Ti)O$_2$ solid solution including srilankite: evolution towards tetragonal ZrO$_2$ with increasing Zr. *Phys. Chem. Miner.*, 2005, **32**(7), P. 504–514.

[96] Troitzsch U., Ellis D.J. The ZrO$_2$–TiO$_2$ phase diagram. *J. Mater. Sci.*, 2005, **40**(17), P. 4571–4577.

[97] Schaedler T.A., Fabrichnaya O., Levi C.G. Phase equilibria in the TiO$_2$–YO$_{1.5}$–ZrO$_2$ system. *J. Eur. Ceram. Soc.*, 2008, **28**(13), P. 2509–2520.

[98] Saenko I., Ilatovskaia M., Savinykh G., Fabrichnaya O. Experimental investigation of phase relations and thermodynamic properties in the ZrO$_2$–TiO$_2$ system. *J. Am. Ceram. Soc.*, 2018, **101**(1), P. 386–399.

[99] Andrievsky R.A., Ragulya A.V. *Nanostructured materials*. Moscow, Ed. Center "Academy", 2005, 192 p. [in Russian].

[100] Bae D.-S., Han K.-S., Choi S.-H. Fabrication and microstructure of TiO$_2$–ZrO$_2$ composite membranes. *J. Mater. Sci. Lett.*, 1997, **16**(8), P. 658–660.

[101] Guo H., Zhao S., Wu X., Qi, H. Fabrication and characterization of TiO$_2$/ZrO$_2$ ceramic membranes for nanofiltration. *Microporous Mesoporous Mater.*, 2018, **260**, P. 125–131.

[102] Hwang D.-H., Lee B.-H. Synthesis and Formation Mechanism of ZrTiO$_4$ Gray Pigment. *J. Korean Ceram. Soc.*, 2012, **49**(1), P. 84–89.

[103] Wang C.L., Lee H.Y., Azough F., Freer R. The microstructure and microwave dielectric properties of zirconium titanate ceramics in the solid solution system ZrTiO$_4$–Zr$_5$Ti$_7$O$_{24}$. *J. Mater. Sci.*, 1997, **32**(7), P. 1693–1701.

[104] Vasilevskaya A.K., Almyasheva O.V. Features of phase formation in the ZrO$_2$–TiO$_2$ system under hydrothermal conditions. *Nanosyst.: Phys. Chem. Math.*, 2012, **3**(4), P. 75–81 [in Russian].

[105] Bachina A.K., Almjasheva O.V., Danilovich D.P., Popkov V.I. Synthesis, Crystal Structure, and Thermophysical Properties of ZrTiO$_4$ Nanoceramics. *Russ. J. Phys. Chem. A*, 2021, **95**(8), P. 1529–1536.

[106] Gusarov V.V. Rapid solid-phase chemical reactions. *Russ. J. Gen. Chem.*, 1997, **67**(12), P. 1959–1964 [in Russian].

[107] Almyasheva O.V. Hydrothermal synthesis, structure and properties of nanocrystals and nanocomposites in the ZrO$_2$–Al$_2$O$_3$–SiO$_2$ system: dissertation abstract ... candidate of chemical sciences: 02.00.04, St. Petersburg, 2007, 24 p. [in Russian].

[108] McMurdie H.F., Hall F.P. Phase diagrams for ceramists: Supplement No. 1. *J. Am. Ceram. Soc.*, 1949, **32**(s1), P. 154–164.

[109] Toropov N.A., Galakhov F.Ya. Liquid immiscibility in the ZrO$_2$–SiO$_2$ system. *Izv. Akad. Nauk SSSR, Otd. Khim. Nauk*, 1956, **2**, P. 157–162 [in Russian].

[110] Jones T.S., Kimura S., Muan A. Phase Relations in the System FeO-Fe$_2$O$_3$-ZrO$_2$-SiO$_2$. *J. Am. Ceram. Soc.*, 1967, **50**(3), P. 137–142.

[111] Butterman W.C., Foster W.R. Zircon stability and the ZrO$_2$–SiO$_2$ phase diagram. *Am. Mineral.*, 1967, **52**(5–6), P. 880–885.

[112] Kamaev D.N., Archugov S.A., Mikhailov G.G. Study and Thermodynamic Analysis of the ZrO$_2$–SiO$_2$ System. *Russ. J. Appl. Chem.*, 2005, **78**(2), P. 200–203.

[113] Kwon S.Y., Jung I.-H. Critical evaluation and thermodynamic optimization of the CaO-ZrO$_2$ and SiO$_2$-ZrO$_2$ systems. *J. Eur. Ceram. Soc.*, 2017, **37**(3), P. 1105–1116.

[114] Al'myasheva O.V., Gusarov V.V. Nucleation in media in which nanoparticles of another phase are distributed. *Dokl. Phys. Chem.*, 2009, **424**(2), P. 43–45.

[115] Almjashev V.I., Gusarov V.V., Khabensky V.B. USiO$_4$ stability analysis. *Technologies for ensuring the life cycle of nuclear power plants*, 2020, **2**(20), P. 80–97 [in Russian].

[116] Pena P., De Aza S. El Sistema ZrO$_2$–SiO$_2$–TiO$_2$. *Bol. Soc. Esp. Cerám. Vidr.*, 1976, **15**(2), P. 93–95.

[117] Sugai M., Fujimori K., Sahara R., Hirano S., Somiya S. Phase Relations in the system ZrSiO$_4$–TiO$_2$ at temperatures between 1500 and 1700 °C. *J. Ceram. Soc. JAPAN*, 1974, **82**(8), P. 447–453.

[118] Phase Equilibria Diagrams Online Search system by NIST ACerS. URL: https://phaseonline.ceramics.org/ped_figure_search (date of access: 01.03.21).

[119] Mazurin O.V., Gusarov V.V. The Future of Information Technologies in Materials Science. *Glass Phys. Chem.*, 2002, **28**(1), P. 50–58.

[120] Information-analytical system for phase diagrams and properties of refractory oxides. URL: http://chemdm.ru/index.php/PhDIAS (date of access: 01.03.21).